

Variation after full projection with triaxially deformed nuclear mean field

Zao-Chun Gao,^{1,2} Mihai Horoi,³ and Y.S. Chen¹

¹*China Institute of Atomic Energy, Beijing 102413, China*

²*State Key Laboratory of Theoretical Physics, Institute of Theoretical Physics, Chinese Academy of Sciences, Beijing 100190, China.*

³*Department of Physics, Central Michigan University, Mount Pleasant, Michigan 48859, USA*

(Dated: September 11, 2015)

We implemented a variation after projection (VAP) algorithm based on a triaxially deformed Hartree-Fock-Bogoliubov vacuum state. This is the first projected mean field study that includes all the quantum numbers (except parity), i.e., spin (J), isospin (T) and mass number (A). Systematic VAP calculations with JTA -projection have been performed for the even-even sd -shell nuclei with the USDB Hamiltonian. All the VAP ground state energies are within 500 keV above the exact shell model values. Our VAP calculations show that the spin projection has two important effects: (1) the spin projection is crucial in achieving good approximation of the full shell model calculation. (2) the intrinsic shapes of the VAP wavefunctions with spin projection are always triaxial, while the Hartree-Fock-Bogoliubov methods likely provide axial intrinsic shapes. Finally, our analysis suggests that one may not be possible to associate an intrinsic shape to an exact shell model wave function.

PACS numbers: 21.60.Jz, 21.60.Cs, 21.10.Hw

I. INTRODUCTION

Hartree-Fock-Bogoliubov (HFB) method has been very successful in describing the global properties of the ground states throughout the whole nuclear region. As a mean field method, HFB breaks the symmetries of the nuclear system, and can be used to study the intrinsic shapes. The HFB calculations with Gogny force show that almost all the calculated 1712 nuclei have axially symmetric HFB minima[1].

Projection can be done on a HFB vacuum to recover the symmetries that the Hamiltonian obeys. To test the quality of the projected wavefunctions, one can compare them with the exact shell model ones using a common Hamiltonian. HFB and variation after projected HFB calculations with shell model Hamiltonians have been reported by several authors [2–5]. For those calculations without projection, the HFB vacuum states are often assumed to be axially symmetric [4]. Indeed, we will see below that all the calculated HFB minima in sd -shell nuclei, except ^{24}Mg , are exactly axial with the USDB Hamiltonian [6].

However, if one performs the variation of the projected HFB vacuum, usually called variation after projection (VAP) [7], it is likely that the intrinsic shape may changes due to the inclusion of beyond mean field correlations. One typical example is the ground state of ^{32}Mg , which is predicted to be spherical at the mean field level [8], but it turns out to have a quadrupole deformation when the correlations associated with the restoration of the broken rotational symmetry are considered [9]. Another example is ^{56}Ni , whose ground state is spherical at the mean field level, but is slightly deformed when performing the projected energy surface calculation [10].

Moreover, the triaxial (γ) degree of freedom plays important roles on the low-lying collective dynamics in this

mass region [11]. In ^{24}Mg the possibility of the triaxial deformation in the ground state was discussed for decades [12–14], and it is still being used as the testing ground for modern theories involving angular momentum (spin) projection [15–17].

In this work, we perform VAP calculations of the even-even sd -shell nuclei using the USDB Hamiltonian. Here, we allow the γ degree of freedom in the HFB transformation. The shell model Hamiltonian conserves the spin (J), isospin (T), as well as the mass number (A). Hence a complete projection should recover all J , T , and A quantum numbers. This is generally very much time-consuming because of the 7-dimensional integration (3 for J , 3 for T , and 1 for A). Presently, we can only carry out such extensive studies in the sd shell. For efficiency, we use the new techniques of Refs. [18–20] to evaluate the kernels for projections.

II. THE VAP METHOD

From a randomly chosen HFB vacuum state $|\Phi_0\rangle$, one can construct a new HFB vacuum state $|\Phi\rangle$ using the Thouless theorem [7]. Namely,

$$|\Phi\rangle = \mathcal{N} e^{\frac{1}{2} \sum_{\mu\nu} d_{\mu\nu} a_{\mu}^{\dagger} a_{\nu}^{\dagger}} |\Phi_0\rangle, \quad (1)$$

where d is a skew symmetric matrix, and \mathcal{N} is the normalization factor. The triaxiality of the HFB vacuum can be treated similar to Ref. [21] so that the $Q_{2\pm 1}$ components of the quadrupole moment vanish.

Projecting $|\Phi\rangle$ onto good quantum numbers J , T , and A one gets the so called JTA -projection (similarly, TA -projection for T , A , etc.). One can evaluate the JTA -projected energy,

$$E_{JTA} = \sum_{MKM_TK_T} f_{MM_T}^* f_{KK_T} \langle \Phi | \hat{H} P_{MK}^J P_{M_TK_T}^T P^A | \Phi \rangle, \quad (2)$$

where P_{MK}^J , $P_{M_T K_T}^T$ and P^A are the spin, isospin and mass number projection operators, respectively. The isospin projection operator is similar to the spin projection operator but in the isospin space. E_{JTA} and the corresponding coefficients f_{KK_T} are obtained by solving

$$\sum_{KK_T} \langle \Phi | (\hat{H} - E_{JTA}) P_{MK}^J P_{M_T K_T}^T P^A | \Phi \rangle f_{KK_T} = 0, \quad (3)$$

with f_{KK_T} satisfying

$$\sum_{MK M_T K_T} f_{MM_T}^* f_{KK_T} \langle \Phi | P_{MK}^J P_{M_T K_T}^T P^A | \Phi \rangle = 1. \quad (4)$$

One can also calculate E_{TA} with TA -projection by simply removing the spin projection from Eqs. (2-4). For the A -projection, the corresponding energy, E_A , is reduced to

$$E_A = \frac{\langle \Phi | \hat{H} P^A | \Phi \rangle}{\langle \Phi | P^A | \Phi \rangle}. \quad (5)$$

Without any projection, we define

$$E_{HFB} = \langle \Phi | \hat{H} | \Phi \rangle. \quad (6)$$

It is natural that one may consider the neutron (N) and proton (Z) projection, as has been done in Refs. [2, 5]. However, this is essentially the same as the $T_Z A$ -projection ($T_Z = (N - Z)/2$). Here, we prefer to take TA -projection to recover the total isospin symmetry.

VAP calculations can be performed by changing the d matrix in Eq.(1). Here, we impose the following restrictions for the d matrix: (1) d is real, (2) keeping the time reversal symmetry, and (3) no mixing between neutron and proton in the HFB transformation. Therefore the total number of free VAP parameters for sd -shell is reduced to $N_{VAP} = 42$. In practice we start with $d = 0$ and with Nilsson+BCS vacuum states $|\Phi_0\rangle$ obtained with randomly chosen quadrupole parameters [10].

To extract the intrinsic shape, the quadrupole moment and the triaxial degree of freedom, Q and γ , are defined such that

$$Q \cos \gamma = \langle \Psi | \sqrt{\frac{16\pi}{5}} \frac{r^2}{b^2} Y_{20} | \Psi \rangle, \quad (7)$$

$$Q \sin \gamma = \langle \Psi | \sqrt{\frac{16\pi}{5}} \frac{r^2}{b^2} \frac{1}{\sqrt{2}} (Y_{22} + Y_{2-2}) | \Psi \rangle, \quad (8)$$

where b is the harmonic oscillator length. $|\Psi\rangle$ refers to an intrinsic state, which may have different forms. Explicitly, we define,

- (1) Q_{HFB} and γ_{HFB} for $|\Psi\rangle = |\Phi\rangle$,
- (2) Q_A and γ_A for $|\Psi\rangle = \frac{P^A |\Phi\rangle}{\sqrt{\langle \Phi | P^A | \Phi \rangle}}$, and
- (3) Q_{TA} and γ_{TA} for $|\Psi\rangle = \sum_{K_T} f_{K_T} P_{M_T K_T}^T P^A | \Phi \rangle$,

TABLE I: Results of the VAP-A calculations for ^{24}Mg . We perform the VAP calculations for several times. Each time we start with different $|\Phi_0\rangle$ states. The numbers in the first column denote different $|\Phi_0\rangle$ states. The second column shows the converged energy E_A^* . Quantities in other columns are calculated with the converged $|\Phi\rangle$ vacua. Energies are in MeV.

$ \Phi_0\rangle$	E_A^*	Q_A	$\gamma_A(^{\circ})$	E_{HFB}	Q_{HFB}	$\gamma_{HFB}(^{\circ})$	$\langle \hat{A} \rangle$
1	-81.358	18.284	10.05	-81.008	18.005	9.46	8.110
2	-81.358	18.284	130.05	-90.178	18.371	128.94	9.013
3	-81.358	18.284	-109.95	-82.684	18.120	-110.61	8.259
4	-81.358	18.284	10.05	-79.720	17.905	9.05	8.000

III. VAP CALCULATIONS FOR ^{24}Mg

When performing the energy variation, one may find that there might be more than one energy minima. Therefore, the energy variation should be calculated several times with different starting $|\Phi_0\rangle$ states which are randomly chosen. We then identify the lowest minimum, and denote it with E^* . Here and below, we only discuss the results corresponding to E^* .

In the present work, we adopt the USDB Hamiltonian [6]. The HFB energy for ^{24}Mg is $E_{HFB}^* = -80.965$ MeV with the constraints $\langle \Phi | \hat{N} | \Phi \rangle = N$ and $\langle \Phi | \hat{Z} | \Phi \rangle = Z$. This is the only sd -shell nucleus for which the HFB calculation gives a non-axial shape with $Q_{HFB}^* = 18.659$ and $\gamma_{HFB}^* = 11.96^{\circ}$ (here and below the Q^* and γ^* are the shape parameters that can be associated with the absolute minimum for some VAP choice). Let's first do the simplest VAP with only A -projection (called VAP-A). Since the particle number is already projected out, it might be unnecessary to impose a constraint to the average particle number of the HFB vacuum. To check this conjecture, we start from several different $|\Phi_0\rangle$ states and perform VAP-A. The results for few selected $|\Phi_0\rangle$ choices are shown in Table I. One can see that the VAP-A energies are identical ($E_A^* = -81.358$ MeV). However, the corresponding E_{HFB} , Q_{HFB} , γ_{HFB} and $\langle \hat{A} \rangle \equiv \langle \Phi | \hat{A} | \Phi \rangle$ appear randomly. This means that the converged vacua $|\Phi\rangle$ are not unique, but correspond to the same A -projected state. The Q_A values are the same, and although the γ_A values look different, they actually represent the same shape but with different orientations. Therefore, one can adopt the values $Q_A^* = 18.284$ and $\gamma_A^* = 10.05$ to define the shape of the VAP-A minimum. If one imposes $\langle \hat{A} \rangle = A = 8$, we still have $E_A^* = -81.358$ MeV, now the converged $|\Phi\rangle$ vacuum becomes unique, with $E_{HFB} = -79.720$, $Q_{HFB} = 17.905$, and $\gamma_{HFB} = 9.05^{\circ}$ (see the last line in Table I). However, for the VAP with TA -projection, the situation becomes a little different.

VAP calculations with TA -projection (called VAP-TA) are listed in Table II. Unlike VAP-A, even if one imposes $\langle \hat{A} \rangle = A = 8$ for ^{24}Mg , the converged $|\Phi\rangle$ is still not unique as the E_{HFB} energy appears randomly. Moreover, the E_A energy is not unique either. Interestingly, after

TA -projection, those different $|\Phi\rangle$ vacuum states have exactly the same projected energy $E_{TA}^* = -82.831(\text{MeV})$ and the same $Q_{TA} = 17.295$. Therefore, we can associate the shape parameter corresponding $Q_{TA}^* = Q_{TA} = 17.295$ to this projected minimum. Similarly, we found (after rotation) $\gamma_{TA}^* = \gamma_{TA} = 0.09^\circ$, which describes an almost axial-shape. One can conclude that only Q_{TA} and γ_{TA} are meaningful in describing the shape of the VAP- TA projected state.

A complete symmetry restoration is the JTA -projection. VAP results with JTA -projection (called as VAP- JTA) are shown in Table III. All the converged E_{JTA}^* energies are -86.919 MeV , significantly closer to the shell model result $E_{SM} = -87.105 \text{ MeV}$. Again, both E_A and E_{HFB} in Table III can not be uniquely determined, even if one enforces the $\langle \hat{A} \rangle = A$ constraint. Fortunately, with the additional spin projection, all E_{TA} values are found to be -79.879 MeV , and similarly the corresponding shape is described by $Q_{TA} = 19.057$ and $\gamma_{TA} = 16.96^\circ$. Therefore, the quantities that can be associated with the shape of VAP- JTA wavefunction should also be $Q_{JTA}^* = Q_{TA} = 19.057$ and $\gamma_{JTA}^* = \gamma_{TA} = 16.96^\circ$.

One can study the shape evolution of ^{24}Mg from HFB to VAP- JTA . In VAP- TA , Q_{TA}^* looks smaller than Q_{HFB}^* in HFB, and γ_{TA}^* tends to be close to zero (axial shape). However in VAP- JTA , Q_{JTA}^* is larger than the Q_{HFB}^* in HFB, and γ_{JTA}^* tends to describe a triaxial shape. This triaxiality in VAP- JTA , in comparison with VAP- TA , is likely caused by the spin projection. To determine if this phenomenon is more general, we performed systematic VAP calculations for a larger number of even-even sd -shell nuclei.

IV. VAP CALCULATIONS FOR EVEN-EVEN sd -SHELL NUCLEI

VAP calculations have been performed for the ground states of even-even sd -shell nuclei. The calculated energies relative to the shell model ones are shown in Figure 1a. The numerical results are given in Table IV. Here, we didn't include the Oxygen isotopes and the $N = 20$ isotones because their VAP- JTA energies are exactly the same as the shell model results (E_{SM}). This special case is discussed below. The VAP- JTA energies are much lower than those of HFB and VAP- TA . Moreover, The VAP- JTA energies for ^{20}Ne , ^{28}Ne , and ^{36}Ar nuclei are exactly the same as the shell model results (see also Figure 1b). This can be understood by comparing the number of VAP parameters, N_{VAP} , with the shell model dimension, N_{JT} (the total number of the independent basis states with good JT). Here, $N_{VAP} = 42$. The N_{JT} values with $J = 0$ and $T = 0$ for both ^{20}Ne and ^{36}Ar are only 21. For ^{28}Ne , N_{JT} for $J = 0$ and $T = 4$ is 43. It looks that when N_{JT} is less than, or close to N_{VAP} , then the VAP- JTA energy is likely to be the same as the shell model one. Indeed, for all even-even oxygen isotopes and

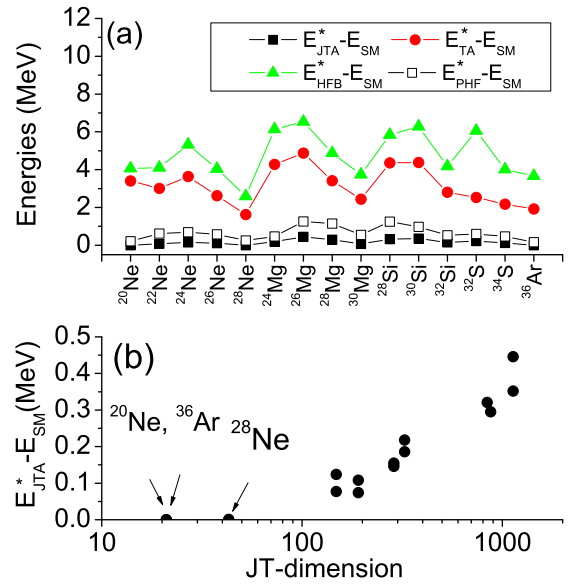


FIG. 1: (Color online) (a) Calculated ground state energies relative to the shell model results, E_{SM} . (b) Relative VAP- JTA energy, $E_{JTA}^* - E_{SM}$, versus the shell model dimension, N_{JT} , in JT subspace.

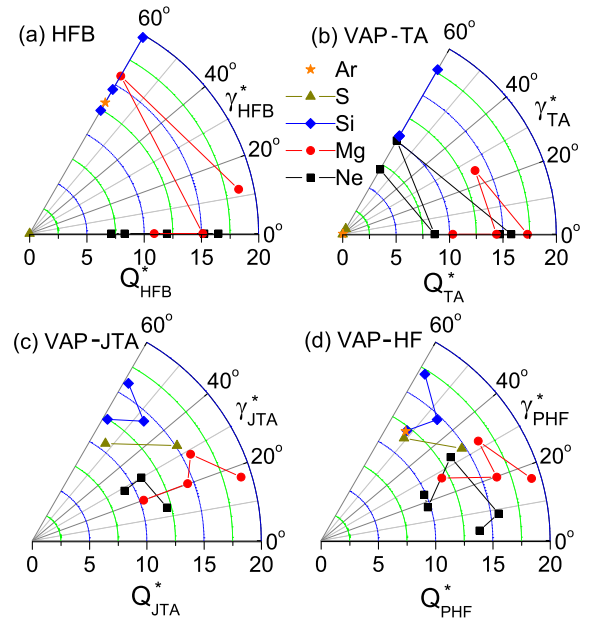


FIG. 2: (Color online) Quadrupole moments Q and γ values for (a) HFB vacuum states, (b) VAP- TA states, (c) VAP- JTA states and (d) VAP-HF states which is based on a Slater determinant.

for the $N = 20$ isotones, for which $N_{JT} \leq N_{VAP}$, we have obtained $E_{JTA}^* = E_{SM}$. In Figure 1b, one can also see that the energy difference $E_{JTA}^* - E_{SM}$ increases with N_{JT} . The largest $E_{JTA}^* - E_{SM} = 0.446 \text{ MeV}$ is obtained for ^{26}Mg , corresponding to the largest $N_{JT} = 1132$.

The quadrupole moment and the γ degree of freedom

TABLE II: Similar to Table. I but for the VAP-TA calculations. $\langle A \rangle = 8$ is imposed.

$ \Phi_0\rangle$	E_{TA}^* (MeV)	Q_{TA}	$\gamma_{TA}(^{\circ})$	E_A (MeV)	Q_A	$\gamma_A(^{\circ})$	E_{HFB} (MeV)	Q_{HFB}	$\gamma_{HFB}(^{\circ})$	$\langle A \rangle$
1	-82.831	17.295	-119.91	-75.826	16.376	-118.62	-74.921	15.755	-118.23	8.000
2	-82.831	17.295	0.09	-74.402	16.167	2.47	-73.909	15.563	3.06	8.000
3	-82.831	17.295	120.09	-76.633	16.526	120.09	-75.525	15.897	120.08	8.000

TABLE III: Similar to Table. I but for the VAP-JTA calculations. $\langle A \rangle = 8$ is imposed.

$ \Phi_0\rangle$	E_{JTA}^* (MeV)	E_{TA} (MeV)	Q_{TA}	$\gamma_{TA}(^{\circ})$	E_A (MeV)	Q_A	$\gamma_A(^{\circ})$	E_{HFB} (MeV)	Q_{HFB}	$\gamma_{HFB}(^{\circ})$	$\langle A \rangle$
1	-86.919	-79.879	19.057	-16.964	-75.600	17.482	-20.225	-73.781	16.230	-23.772	8.000
2	-86.919	-79.879	19.057	-16.963	-75.641	17.510	-20.119	-73.830	16.264	-23.604	8.000
3	-86.919	-79.879	19.057	-16.963	-75.644	17.520	-20.068	-73.845	16.281	-23.506	8.000

can be extracted using Eqs. (7) and (8). In Fig. 2a, the γ_{HFB}^* values in HFB are either 0° or 60° , except $\gamma_{HFB}^* = 12^{\circ}$ for ^{24}Mg , thus supporting the conclusion that HFB likely presents axially deformed shapes. In Fig. 2b, the shapes in VAP-TA calculations still remain axially symmetric, except for ^{26}Mg , which has $\gamma_{TA}^* = 25.7^{\circ}$. Quite differently, the γ_{JTA}^* values in the VAP-JTA calculations (Fig. 2c) show that all these nuclei are non-axial without exception. Comparing these results with those of Fig. 2a, one can conclude that the triaxiality in VAP-JTA is definitely a beyond mean-field effect, which is likely to be a universal phenomenon. Fig. 2b, however, excludes the possibility that the isospin projection and the mass projection lead to triaxiality. Thus, the only possible cause of the triaxiality is the beyond mean-field spin projection.

To study directly the effect of spin projection, one can start from a Hartree-Fock (HF) Slater determinant (SD) and perform VAP calculations with only spin projection (called VAP-HF). The converged energies, E_{PHF}^* , relative to E_{SM} , are shown in Fig. 1a. The results show that VAP-HF is better than VAP-TA, and quite close to the VAP-JTA. The quadrupole moment Q_{PHF}^* and γ_{PHF}^* corresponding to E_{PHF}^* can be calculated using Eqs. (7) and (8) with $|\Psi\rangle$ replaced by the converged SD. These quantities are uniquely determined, and are shown in Fig. 2d. Again, all the γ_{PHF}^* values are distributed in the interval $(0^{\circ}, 60^{\circ})$, which is very similar to Fig. 2c. Therefore, we could conclude that VAP results that include spin projection can always be associated with intrinsic states having triaxial deformation.

One more interesting phenomenon, however, is related to the VAP-JTA calculations for ^{20}Ne , ^{28}Ne , and ^{36}Ar . We have shown above that the E_{JTA}^* energies of these nuclei are the same as the exact shell model results. Surprisingly, the corresponding Q_{TA} and γ_{TA} values are not unique, which is quite different from other nuclei with $E_{JTA}^* > E_{SM}$. For example, the results for ^{20}Ne are shown in Table V. With the same converged $E_{JTA}^* = -40.472\text{MeV}$, one can clearly see that starting with different initial states $|\Phi_0\rangle$, the result for Q_{TA} and γ_{TA} could be different. These results indicate that it may

not be possible to associate an unique intrinsic deformation with an exact eigenstate of the Hamiltonian.

V. SUMMARY

We implemented an algorithm that performs variation after projection (VAP) on spin, isospin, and mass number of a triaxially deformed Hartree-Fock-Bogoliubov vacuum state. This is the first projected mean field study that includes all these quantum numbers.

We start from a randomly chosen HFB vacuum state and carry out VAP calculations for ^{24}Mg in *sd*-shell with various projections. In the VAP-A case the converged solution is independent of the Fermi level (chemical potential). Although the associated HFB vacuum does not have definite quadrupole moment Q_{HFB} and triaxial deformation parameter γ_{HFB} , one can use the unique Q_A and γ_A to describe the intrinsic deformation of the VAP-A state. Similarly, in the VAP-TA calculations, Q_A and γ_A can not be uniquely determined, but Q_{TA} and γ_{TA} are unique and can be associated with the intrinsic deformation of the VAP-TA state. It is not possible to directly define deformation parameters Q and γ for the VAP-JTA wave function, which has the symmetries fully restored, but the Q_{TA} and γ_{TA} calculated with the VAP-JTA vacuum state $|\Phi\rangle$ are also unique, and can be associated with the intrinsic deformation of the VAP-JTA state.

Systematical VAP calculations of even-even *sd*-shell nuclei have been performed using the USDB Hamiltonian. The VAP-JTA energies, E_{JTA}^* , are very close to the shell model results, E_{SM} . Moreover, the relative energy, $E_{JTA}^* - E_{SM}$, increases with the shell model dimension N_{JT} . The shapes described by the HFB minima are always axial. However, with spin projection VAP calculations always produce triaxial shapes. We believe that such triaxiality is an universal phenomenon caused by the beyond mean-field dynamic correlations. Finally, we show that those VAP-JTA states reaching the exact shell model results do not have clearly defined intrinsic shapes.

TABLE IV: Converged energies and associated shape parameters for even-even *sd*-shell nuclei calculated with the USDB Hamiltonian.

Nucleus			VAP-JTA			VAP-TA			HFB			VAP-HF		
	N_{JT}	E_{SM}	E_{JTA}^*	Q_{JTA}^*	γ_{JTA}^*	E_{TA}^*	Q_{TA}^*	γ_{TA}^*	E_{HFB}^*	Q_{HFB}^*	γ_{HFB}^*	E_{PHF}^*	Q_{PHF}^*	γ_{PHF}^*
²⁰ Ne	21	-40.472	-40.472	—	—	-37.069	14.7	0.0	-36.404	15.3	0.0	-40.265	13.861	3.551
²² Ne	148	-57.578	-57.501	12.1	13.8	-54.572	15.8	0.0	-53.474	16.5	0.0	-56.958	15.675	8.632
²⁴ Ne	287	-71.725	-71.570	11.0	30.1	-68.084	10.1	60.0	-66.402	12.0	0.0	-71.037	13.449	32.786
²⁶ Ne	191	-81.564	-81.465	9.2	28.4	-78.949	8.6	0.0	-77.518	8.3	0.0	-80.988	9.760	17.265
²⁸ Ne	43	-86.543	-86.543	—	—	-84.920	7.0	60.0	-83.949	7.1	0.0	-86.294	9.848	23.934
²⁴ Mg	325	-87.105	-86.919	19.1	17.0	-82.831	17.3	0.0	-80.965	18.7	12.0	-86.636	19.165	16.427
²⁶ Mg	1132	-105.521	-105.075	15.8	28.7	-100.648	13.8	25.7	-98.992	15.9	60.0	-104.264	16.238	32.331
²⁸ Mg	874	-120.500	-120.205	14.5	20.2	-117.091	14.4	0.0	-115.625	15.1	0.0	-119.354	16.306	19.835
³⁰ Mg	191	-130.474	-130.400	10.4	20.0	-128.035	10.3	0.0	-126.735	10.9	0.0	-129.926	11.864	27.322
²⁸ Si	839	-135.860	-135.539	16.1	58.6	-131.501	17.8	60.0	-130.021	19.8	60.0	-134.617	17.116	58.038
³⁰ Si	1132	-154.754	-154.402	14.3	47.0	-150.380	10.6	60.0	-148.475	14.5	60.0	-153.777	14.633	46.167
³² Si	287	-170.519	-170.373	12.5	58.2	-167.721	10.6	60.0	-166.344	12.4	60.0	-169.996	12.175	52.023
³² S	325	-182.452	-182.234	15.1	33.3	-179.925	0.6	60.0	-176.393	0.0	0.0	-181.856	14.681	33.188
³⁴ S	148	-202.504	-202.380	10.6	53.0	-200.331	0.0	0.0	-198.493	0.0	0.0	-202.039	11.496	50.992
³⁶ Ar	21	-230.277	-230.277	—	—	-228.355	0.0	0.0	-226.611	13.2	60.0	-230.112	12.068	52.293

TABLE V: VAP results with JTA projection for ²⁰Ne.

$ \Phi_0\rangle$	E_{JTA}^* (MeV)	E_{TA} (MeV)	Q_{TA}	$\gamma_{TA}^*(^\circ)$
1	-40.472	-28.284	6.314	-45.134
2	-40.472	-30.468	11.873	-124.746
3	-40.472	-27.932	9.876	2.592

Acknowledgments

Z-C. Gao thanks Prof. G. F. Bertsch for fruitful discussions, and Prof. Y. Sun for reading the manuscript. This

work is partly supported by the National Natural Science Foundation of China under Contract No.s 11175258, 11575290, 11321064 and 11275068; the CUSTIPEN (China-U.S. Theory Institute for Physics with Exotic Nuclei) under DOE Grant No. DE-FG02-13ER42025; the Open Project Program of State Key Laboratory of Theoretical Physics, Institute of Theoretical Physics, Chinese Academy of Sciences, China (No.Y5KF141CJ1). M.H. acknowledges the U.S. NSF Grant No. PHY-1404442.

-
- | | |
|---|---|
| <p>[1] J.-P. Delaroche et al., Phys. Rev. C 81, 014303 (2010).
 [2] I. Maqbool, J. A. Sheikh, P. A. Ganai and P. Ring, J. Phys. G 38 045101 (2011).
 [3] R. Rodríguez-Guzmán, Y. Alhassid, and G. F. Bertsch, Phys. Rev. C 77, 064308 (2008).
 [4] L. M. Robledo and G. F. Bertsch, Phys. Rev. C 84, 014312 (2011).
 [5] K.W. Schmid, Prog. Part. Nucl. Phys. 52, 565 (2004).
 [6] B. A. Brown and W. A. Richter, Phys. Rev. C 74, 034315 (2006).
 [7] P. Ring and P. Schuck, The Nuclear Many-Body Problem (Springer Verlag, New York, Heidelberg, Berlin, 1980).
 [8] P.-G. Reinhard, D. J. Dean, W. Nazarewicz, J. Dobaczewski, J. A. Maruhn, and M. R. Strayer, Phys. Rev. C 60, 014316 (1999).
 [9] R. R. Rodríguez-Guzmán, J. L. Egido, and L. M. Robledo, Phys. Lett. B474, 15 (2000); Phys. Rev. C 62, 054319 (2000).
 [10] Zao-Chun Gao, Mihai Horoi, and Y. S. Chen, Phys. Rev. C 80, 034325 (2009).</p> | <p>[11] D. Kurath, Phys. Rev. C 5, 768 (1972).
 [12] W. Koepf and P. Ring, Phys. Lett. B 212, 397 (1988).
 [13] P. Bonche, H. Flocard, and P. H. Heenen, Nucl. Phys. A 467, 115 (1987).
 [14] R. K. Sheline, I. Ragnarsson, S. Åberg, and A. Watts, J. Phys. G 14, 1201 (1988).
 [15] Michael Bender and Paul-Henri Heenen Phys. Rev. C 78, 024309 (2008).
 [16] J. M. Yao, J. Meng, P. Ring, and D. Vretenar Phys. Rev. C 81, 044311 (2010).
 [17] Tomás R. Rodríguez and J. L. Egido Phys. Rev. C 81, 064323 (2010).
 [18] Z.-C. Gao, Q.-L. Hu, Y.S.Chen Phys. Lett. B732, 360 (2014).
 [19] Q.-L. Hu, Z.-C. Gao, Y.S.Chen Phys. Lett. B734, 162 (2014).
 [20] L.-J. Wang, F.-Q. Chen, T. Mizusaki, M. Oi, Y. Sun, Phys. Rev. C 90 (2014) 011303(R)
 [21] K. Hara, Y. Sun, Int. J. Mod. Phys. E 4, 637 (1995).</p> |
|---|---|